A Spring-based Inductive Sensor for Soft and Flexible Robots

Sujit Kumar Sahu, Izadyar Tamadon, Benoit Rosa, Pierre Renaud, Arianna Menciassi

A Spring-based Inductive Sensor for Soft and Flexible Robots

Sujit Kumar Sahu, Izadyar Tamadon, Benoit Rosa, *Member, IEEE*, Pierre Renaud*, *Member, IEEE*, Arianna Menciassi*, *Member, IEEE*

***Abstract*— The development of flexible and soft robots generates new needs in terms of instrumentation, as large encountered deformations require highly stretchable strain sensors. In this regard, we contribute to the adoption of inductive sensors by providing tools to model and exploit them, and showing their relevance experimentally. First, strain estimation based on voltage measurement is proposed. Compared to direct inductance evaluation, the principle is easier to implement and opens the possibility to optimize the measurement performances by tuning the circuit components and interrogation frequency. The possibility of performing a single sensor calibration independently via the elongation mode during strain sensing is outlined. A detailed characterization is then performed which shows that the sensor produces a low hysteresis of 0.1 %, a precision in the order of 0.14 %, and an accuracy of 0.9 %. Finally, two proofs of concept are proposed: I) The integration with a pneumatic artificial muscle (PAM) that demonstrates the added value of the sensor for a model-free precise control of a soft system; II) The closed-loop control of a flexible bending manipulator using the inductive sensor. The performance in the closed-loop control is demonstrated, with a sensing element that is easy to integrate mechanically, strengthening its potential to be used as a structural element as well.**

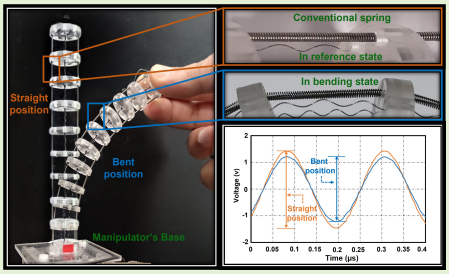

***Index Terms*— Flexible sensor, inductance sensing, stretchable sensor, sensing for soft actuator, sensing for flexible manipulator.**

I. Introduction

SOFT and flexible robots [1]–[4] are gaining popularity due to their potential for solving some major limitations of the conventional robots. In particular, they offer the required deformation capability in elongation and bending for safe deployment in an unstructured environment as encountered typically during medical interventions. Soft robots should be operated accurately and precisely to offer safety and reliability in a medical context. The open-loop control lacks efficiency if external loads act on the robot. However, a mathematical model-based control may be possible for controlling these robots. But even then, a small mismatch between the actual system and model can greatly affect the predictions and overall performance [5]. Thus, the integration of sensors on a robot is essential for a closed-loop operation. The use of traditional sensors such as strain gauges, flex/bend sensors, and encoders may not be efficient, as they do not support the structural compliance of the robot's body, thus limiting its elongation. Hence, internal stretchable sensors are key elements to explore the full functionality of soft and flexible robots.

Stretchable embedded sensors based on the change in electrical resistance were developed in [6] by direct printing and by using conductive liquid microchannels [7]–[9] to measure the strain and curvature of actuators. With an interesting configuration [10], strain sensing was combined with the actuation of the soft actuator through conductive working fluids. Coil-based resistive sensors are also presented in the literature. Tang et al. [11] presented a resistive sensor based on coiled conductive fibers to control the tip angle of a soft actuator. The resistive sensors appear to have several advantages, such as ease of fabrication, high stretchability, and simplicity of design. However, the hysteresis remains significant [12] due to the viscoelastic behavior of the involved elastomeric material.

Capacitive sensors are also getting attention [13]–[15] in the framework of soft and flexible robotics. Legrand et al. [16] proposed a capacitance-based strain sensing method for a braided pneumatic artificial muscle by measuring the capacitance between two replaced conductive braids. Nakamoto et al. [13] proposed a carbon nanotube-based capacitive strain sensor for measuring the contraction of an artificial muscle. Capacitive sensors show less hysteresis, higher linearity, and faster response time, compared to resistive sensors [17]. A major concern still remains; since they are made from elastomeric materials, removing their hysteresis and non-linearities

This work was supported by the ATLAS project. This project has received funding from the European Union's Horizon 2020 research and innovation programme under the Marie Sklodowska-Curie grant agreement No 813782.

Sujit Kumar Sahu, Izadyar Tamadon, and Arianna Menciassi are with the BioRobotics Institute and Department of Excellence in Robotics & AI, Scuola Superiore Sant'Anna, Pontedera, 56025, ITALY, (correspondence e mail: sujitkumar.sahu@santannapisa.it).

Sujit Kumar Sahu, Benoit Rosa, and Pierre Renaud are with the ICube, CNRS, University of Strasbourg - INSA Strasbourg, 67081, France.

∗The authors contributed equally to this work.

is difficult. Miniaturization is also a challenge that they share with resistive sensors.

Miniaturization is one of the motivations for the development of optical fiber sensors. The linear and bending strain of robots can be measured using the modulation of the emitted lights in terms of the change in intensity [18], [19], wavelength [20], phase [21], and polarisation [22]. The change in light intensity was used in [18], [19] to measure the bending, elongation, and compression of the soft actuators. The wavelength-based fiber bragg grating (FBG) sensing technology was implemented in soft and flexible manipulators [23]–[26] for sensing the shape. A complete review of optical fiber sensors was presented in [27]. The combination of high accuracy, miniaturization, and excellent electrical insulation property makes these sensors quite unique. However, the cost and, most importantly, the limited strain range [28], [29] hamper their use in soft and flexible robotics.

Inductive strain sensors have been receiving attention due to their low hysteresis, good stretchability, and excellent signal repeatability [30]–[32]. Several research groups proposed various soft inductive electronics [33]–[35] for strain and tactile sensing that employed silicone as a base substrate. They can be used in flexible and soft robots by attaching them onto the skin. These sensors are useful for proximity and tactile information. However, implementing them in robots that show high elongation remains limited due to their size and shape. As a result, solenoid-type inductance strain sensors were considered several times in the literature. The longitudinal strain of a McKibben structure and bending strain of a bellows-driven continuum manipulator were estimated by measuring the inductance of braided wires [31], [32]. In another application, the exploitation of hollow coils accompanied with an LCR meter unit was demonstrated for measuring the bending angle of a soft actuator [30]. A soft pneumatic actuator with a conventional spring as a built-in displacement sensor was presented in [36]. In this case, the position of the soft actuator was controlled by measuring the oscillation frequency of a Pierce Oscillation Circuit [36]. In the case of a rehabilitation application, a soft solenoidal bend sensor was incorporated into wearable devices by measuring the inductance [37]. In [38], a soft inductive sensor was proposed to estimate the linear displacement of a robotic arm by measuring the differential analog voltage between shape memory alloy springs placed antagonistically, using a custom circuit. On another note, voice coil shape sensors were developed for reconstructing the shape of medical catheters [39]. In this case, the induced voltage between the excitation and sensor coils placed along the catheter was measured to estimate the shape. Thus, inductive sensors show great potential in the strain measurement process. Given their good accuracy and a significant range of inductance change, they were repeatedly considered in the literature for flexible devices. However, specific instrumentation is generally needed to use them. Additionally, the versatility of inductive sensing when different modes of deformation are encountered by a sensor was not discussed. Typically, an actuator in bending or extension alone is considered for a given sensor. Therefore, it is critical to determine whether the same sensor can be integrated into both bending and linear deforming robots without increasing the overall complexity. Furthermore, the behaviour of a coil-type inductive sensor was not characterized in depth. In this paper, four main contributions towards the development of inductive strain sensors have been presented.

First, we propose to consider the strain estimation using a simple voltage measurement instead of performing a direct measurement of inductance. This simplifies the required instrumentation. Meanwhile, we show that the circuit comprised a resistor and a spring as a variable inductor that can be adjusted so that the sensing properties, namely sensitivity and gain, can be optimized by tuning the circuit parameters. Second, we experimentally show that a single calibration of the sensor can be carried out independently via either elongation or bending, or a combination of both. Therefore, the calibration can be used before any integration and still be valid in many devices. Like FBG, the inductive sensors also offer the possibility of estimating the combined elongation and bending of the manipulator using multiple sensors. Third, we conduct a full characterization process for the sensor to elaborate on its hysteresis, stretchability, repeatability, strain rate response, precision, and accuracy. Finally, we show two proofs of concept in which the same inductive sensor is integrated with two different application scenarios. The first one demonstrates the use of the sensor in a soft robot featuring a large strain in elongation. It shows that the sensor can control the soft actuator effectively with acceptable accuracy despite the absence of any physical model. The second one is a tendon-driven bending manipulator. We show that the same sensor can be easily integrated with a high level of compactness, while using the same initial calibration for the device control.

The paper is organized as follows: Section II provides the principle behind inductance sensing and the proposed methodology for the adjustment of the measurement conditions; section III shows the characterization process and experimental results; section IV presents the first proof of concept, comprising a soft module with the integrated sensor and its closed-loop control; section V illustrates the second proof of concept with the closed-loop control of the flexible tendon-driven module; section VI discusses the different benefits and limitations of this sensing method and concludes the paper by describing the scope and implications for future research.

II. Analysis and Optimization of the Strain Measurements

A. Modeling and optimization of the strain sensing principle

The strain sensing we consider here is based on the principle of variable electrical inductance. The sensing element is a conductive coil spring of length l and diameter D built from n turns of a wire. It can be modeled as an inductor L with a parasitic capacitance C. We consider an arrangement where the coil spring is connected to a resistor R in series with an AC voltage source of amplitude V_i and frequency ω. Fig. 1. shows the circuit diagram for the sensor. By neglecting the internal resistance of the spring and considering the deformation, such that the coil spring holds its shape, the voltage across the inductor V_o can be derived in a simple way:

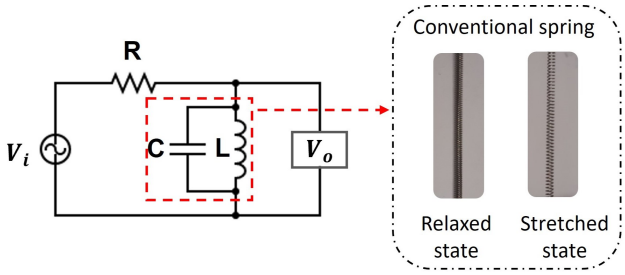

Fig. 1. Modelling of the electrical circuit

$$V_o = \frac{j\omega L}{R(1-\omega^2 LC) + j\omega L} \times V_i \tag{1}$$

The inductance is linked to the area (A), length, and permeability of free space (μ_o), which is given as follows:

$$L = \frac{\mu_o n^2 A}{l} \tag{2}$$

The gain (G) of the circuit can be estimated as:

$$G = \frac{y}{\sqrt{(l-x)^2 + (y)^2}} \tag{3}$$

Where $G = |V_o/V_i|$, $x = \omega^2 \mu_o n^2 AC$, and $y = \omega \mu_o n^2 A/R$.

Both x and y depend on the physical properties of the sensor such as μ_o, A, and C, and that of the electric circuit, ω and R. All of these are considered constant during the measurements. Once the values of x and y are determined, it is then possible to estimate the spring length from the gain.

The parasitic capacitance C is typically very small, with an order of magnitude of $10^{-12}F$ [40], [41]. Therefore, we consider that x is several orders of magnitude smaller than l, which means l-x is always positive. As such, G monotonically decreases when the spring length increases.

Two criteria are of particular importance when characterizing the sensing performance. The first one is obviously the derived gain value G. The second one is the sensitivity S, which can be computed as the derivative of the gain G with respect to the sensor length:

$$S = \frac{dG}{dl} = -\frac{y(l-x)}{((l-x)^2 + y^2)^{1.5}} \tag{4}$$

Achieving a direct measurement of the voltage instead of the inductance makes it possible to adjust the measuring conditions to optimize the sensing performance. The value of the resistance R of the circuit and the frequency of the AC input ω constitute two adjustable parameters for satisfying gain and sensitivity values simultaneously.

Equation (3) shows that the gain approaches 1 when y tends to infinity. This is only possible when ω becomes as big as possible and R is as small as possible. However, from equation (4), it can be observed that the sensitivity of the circuit approaches 0 when ω tends to infinity. The contradictory influence on gain and sensitivity makes it necessary to identify a method for the optimization of measurement conditions. In this regard, we propose a two-step procedure.

In the first step, the resistance value is selected. Reducing the resistance to a small value will indeed increase the gain, but it may also increase the amount of current drawn and induce unwanted heating effects. Setting a high value for the resistance will decrease the gain, thereby limiting the effectiveness of the strain measurement process. Hence, we suggest setting the resistance to a "middle point" value "chosen qualitatively" by considering the above aspects. This will be illustrated in the next section. The selected value needs to be verified afterward, at the end of the second step.

In the second step, the selection of frequency is formulated as an optimization problem. The optimal frequency f^* is defined by:

$$\omega^* = 2\pi f^* = argmax[S(w)] \tag{5}$$

Where ω is angular frequency

Once f^* is computed, the gain value is verified, and steps 1 and 2 will be repeated, if needed.

TABLE I
SPRING SPECIFICATIONS (APPROX. VALUES)

Properties	Spring 1	Spring 2
Length of the spring (l) [mm]	100	100
Diameter of the spring (D) [mm]	1.15	0.85
Wire diameter of spring (d) [mm]	0.1	0.1
Number of turns (n)	650	680
Parasitic capacitance (C) [pF]	1.38	1.14
Theoretical optimum frequency [MHz]	4.5	7.2

B. Application of the optimization method

As an illustration, we consider two springs whose properties are as given in Table 1. The method was initially implemented in spring 1. Using the considerations presented above, the resistance value was set to 220 Ω as a middle point. Then, the optimal frequency was computed using the properties listed in Table 1. As a result, the optimal frequency reached 4.5 MHz when the frequency was swept from 1 kHz to 25 MHz.

For verifying and illustrating the influence of the measurement conditions, all the parameters were substituted in Equation (4) to get the relationship between the sensitivity, frequency, and length of the sensor. Next, the sensitivity was observed by varying the frequency from 1 kHz to 25 MHz and the length from 0.1 m to 0.2 m. Fig. 2a shows the relationship in which the X-axis and Y-axis show the circuit frequency and length of the sensor, respectively, while the Z-axis shows the sensitivity of the sensor. From the figure, it can be observed that the sensitivity follows a saddle trend, i.e., the sensitivity increases up to a certain frequency and then decreases afterward. The point where the sensitivity of the sensor becomes maximum can be found as 4.5 MHz.

In order to visualize the coupled impact of the frequency and resistance, the same procedure was followed and the evolution of the gain and sensitivity was computed by varying the circuit resistance from 20 Ω to 1000 Ω. The gain and maximum sensitivity of the sensor are plotted as functions of the resistance in Fig. 2b. The sensitivity varies only slightly, with a 14% evolution. The resistance value is then not critical, and the selected value is seen suitable. However, setting the resistance to a higher value will reduce the gain, thus making the strain measurement process less effective. From

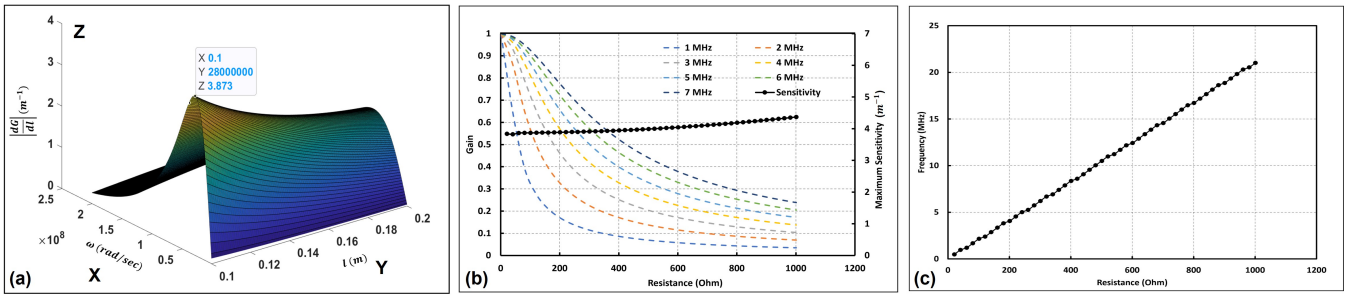

Fig. 2. (a) Theoretical relationship between sensitivity w.r.t. input frequency and length; (b) relationship between the circuit gain and maximum sensitivity of sensor w.r.t circuit resistance; (c) relationship between input frequency for maximum sensitivity w.r.t circuit resistance.

the plot between the frequency at which maximum sensitivity occurs with respect to resistance (Fig. 2c), it should be noted that the optimal frequency f^* increases by increasing the resistance. For instance, the frequency reaches 21 MHz when the resistance value is 1KΩ. In terms of instrumentation, this adds a constraint to having an adequate sampling rate and measurement accuracy at high frequencies. Moreover, this may require a high-end input supply for generating high frequency.

As a complementary step, beyond the proposed method for set-up selection (Fig. 3a), we investigated the frequency for maximum sensitivity experimentally. Spring 1 was connected to a 220 Ω resistor and a 5V peak-to-peak (P-P) AC sinusoidal voltage was supplied from a function generator (33220A, Agilent Technologies, USA). The voltage in the inductor was measured using an oscilloscope (MSO7034B, Agilent Technologies, USA). All the acquisitions were synchronized using LabVIEW. Spring 1 was connected to the setup as shown in Fig. 3b and elongated up to a 40% strain with a rate of 1 mm/s using a linear motorized stage setup (PI, USA), thus helping determine the relationship between gain of the sensor and strain data. The process was repeated for input frequencies between 0.5 and 16 MHz. Finally, the sensitivity of the sensor was estimated by calculating the slope of each curve and plotted against varying frequencies.

Fig. 3c shows the comparison between the experimental and theoretical evolution of the sensitivity-frequency relationship for spring 1. The results are consistent in terms of sensitivity variation, even if the maximum senisivity value is experimentally higher than the computed value. It should be noted that the computed and measured frequencies for maximum sensitivity are in good accordance.

To check whether the proposed method can be applied with other springs, the procedure was followed for the second spring that is listed in Table 1 as well with the same circuit resistance value. The results from calculating the best frequency are as shown in Fig. 3d and highlight the alignment of the theory with the experiment. For high frequencies, however, the estimated values differ from the experimental results. The variation in these curves might be due to the considerations made in establishing the sensitivity expression (4), such as neglecting the internal electrical resistance and the variation in the pitch and diameter of the sensor. Regardless, the method seems applicable and helpful in setting the measurement conditions.

C. Impact of deformation mode on the sensor's characteristics

The derivation of the gain and sensitivity was performed by considering the spring length variation. This variation can be due to a pure linear elongation with coil loops remaining parallel, or bending, or a combination of these deformation modes (Fig. 4a) when the sensor is placed in a flexible manipulator. Having to calibrate the sensor for each type of deformation is time-consuming. It can also be a constraint if the deformation mode changes during the use of the flexible device, especially if an external contact occurs.

An experimental investigation was then carried out to verify if the calibration can be performed only once, to accomplish the measurements of the spring's curvilinear length. The experimental setup comprised four adjustable semi-circular plates of different radii and the linear stage (Fig. 4b). One end of spring 1 was fixed to one end of the semi-circular plate while the other end was connected to the stage setup using a stainless-steel thread. Given its intended use in soft and flexible devices for medical applications, a 40% elongation was applied to the sensor by moving the stage setup. Next, the acquired elongation and P-P voltage were used to find the plot between them. The experiment was repeated for four arbitrary radii (50 mm, 60 mm, 70 mm, and 80 mm). Subsequently, the curves generated from this process were compared with the curve produced by the sensor for a linear elongation of the same amplitude using the setup given in Fig. 3.

The comparison between the experimental results is displayed in Fig. 4c. It shows that the gain change remains almost constant, i.e., 0.1% variation, irrespective of the radius of curvature. It concludes that the sensing capability is independent of the radius and exclusively depends on the amount of strain applied. Moreover, the experimental result shows that the elongation due to linear and bending strain produces similar results. Thus, a single calibration can be performed for a given spring before any integration and used for finding the strain, given the system's type i.e. bending or linear. However, if multiple strain modes are involved, the difference between various strain modes can be identified and measured using multiple sensors.

III. Characterization of the Sensor

A detailed characterization process was conducted to understand the achievable performance of this type of sensor. The

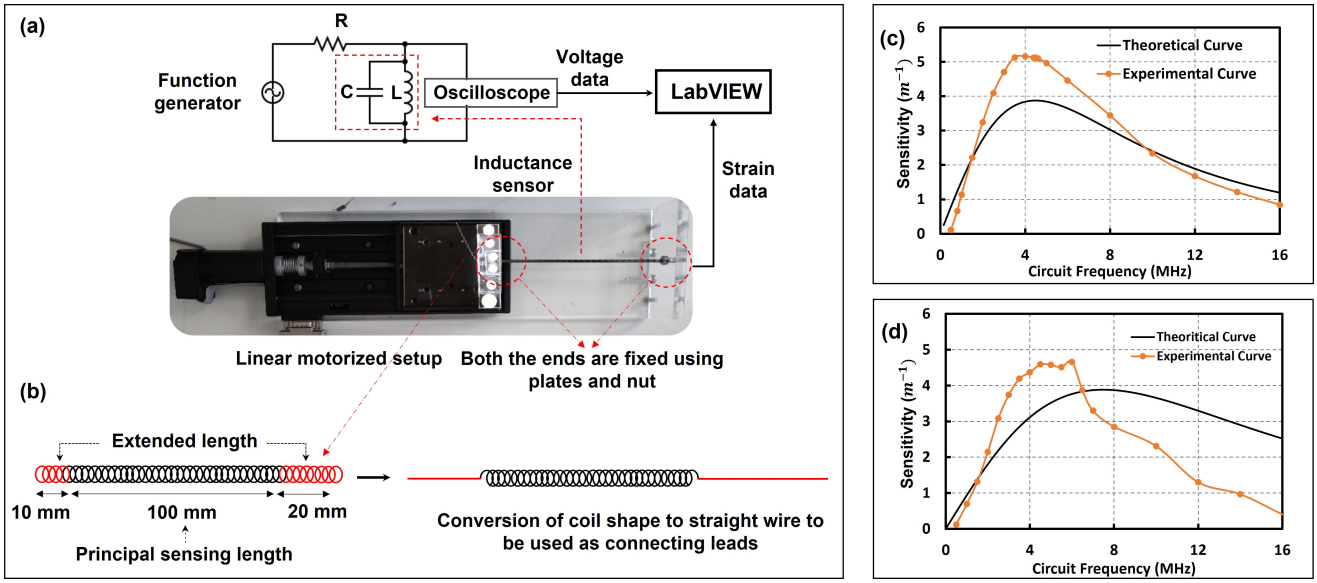

Fig. 3. (a) Experimental measurement setup; (b) sensor realization from the commercial spring; comparison between experimental results with theory for (c) 1.15 mm diameter spring; (d) 0.85 mm diameter spring.

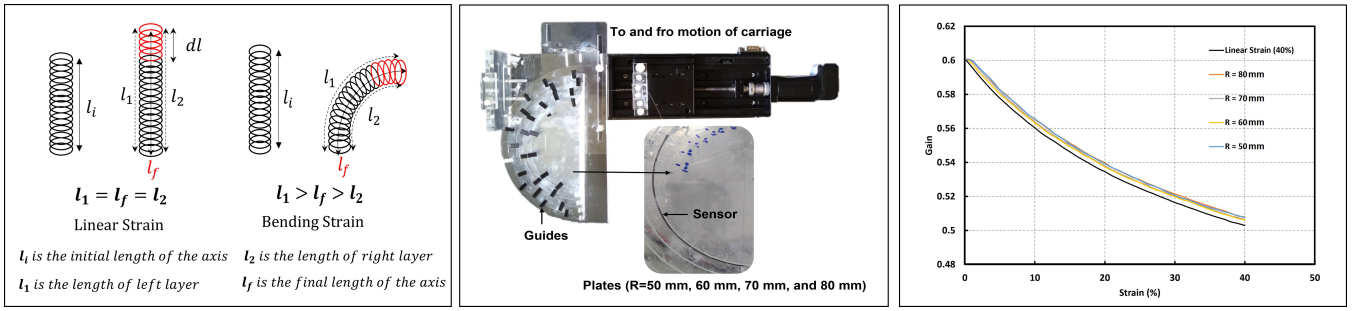

Fig. 4. (a) Schematic representation of the spring with different applied strains; (b) setup for investigating the bending; (c) comparison of the gain and strain relationship for the bending and linear strains.

evolution of gain, as well as the hysteresis during repetitive loading, was elaborated. Moreover, the strain rate effect to consider the impact of elongation speed, precision, and accuracy were considered. Spring 1 was used for the testing and was connected to the setup described in the previous section (Fig. 3a). The input signal frequency and voltage magnitude were set to 4.5 MHz and 5 V, respectively, following the conclusions of section II(B).

A. Evolution of gain and the presence of hysteresis during repetitive loading

Initially, the sensor was subjected to a repetitive loading by applying an 80% strain using the stage setup shown in Fig. 3a. Next, the P-P values of the output voltage across the sensor were acquired regularly for the forward and backward motions. This was repeated for 100 cycles. Next, the resulting gain and time were plotted to investigate the gain change in each cycle. Fig. 5a shows the relationship between the gain for each cycle and time. The difference between the gain change for the first and last cycle was calculated as 0.03%. This showed that the gain change remained almost the same for each cycle during repetitive loading.

The hysteresis produced by the sensor during the repetitive loading was estimated by plotting the acquired gain with respect to the corresponding strain. Fig. 5b shows the electrical hysteresis of the sensor for 100 cycles at 80% strain. When the hysteresis of the sensor was calculated, it produced a mean hysteresis of 0.1% with a standard deviation of 0.023%. This shows that the sensor exhibits low hysteresis, compared to resistive sensors [11], [12]. The gain change for each cycle is also repetitive in nature, since the variation is only 0.03 % for 100 cycles.

B. Effects of strain rates on the sensing behaviour

The electrical hysteresis of the sensor for 80% elongation was estimated by varying the strain rates from 0.1 to 10 mm/s. The curves at different strain rates (Fig. 5c) remained almost similar and produced a mean hysteresis of 0.1% which had a standard deviation of 0.09%. From Fig. 5c, it was observed that the hysteresis varies at different strain rates. However, the values remained small at each strain rate. As the impact of speed on the hysteresis behaviour of the sensor is limited, it can be an interesting solution for a wide range of applications moving at various speeds ranging from 0.1 to 10 mm/s.

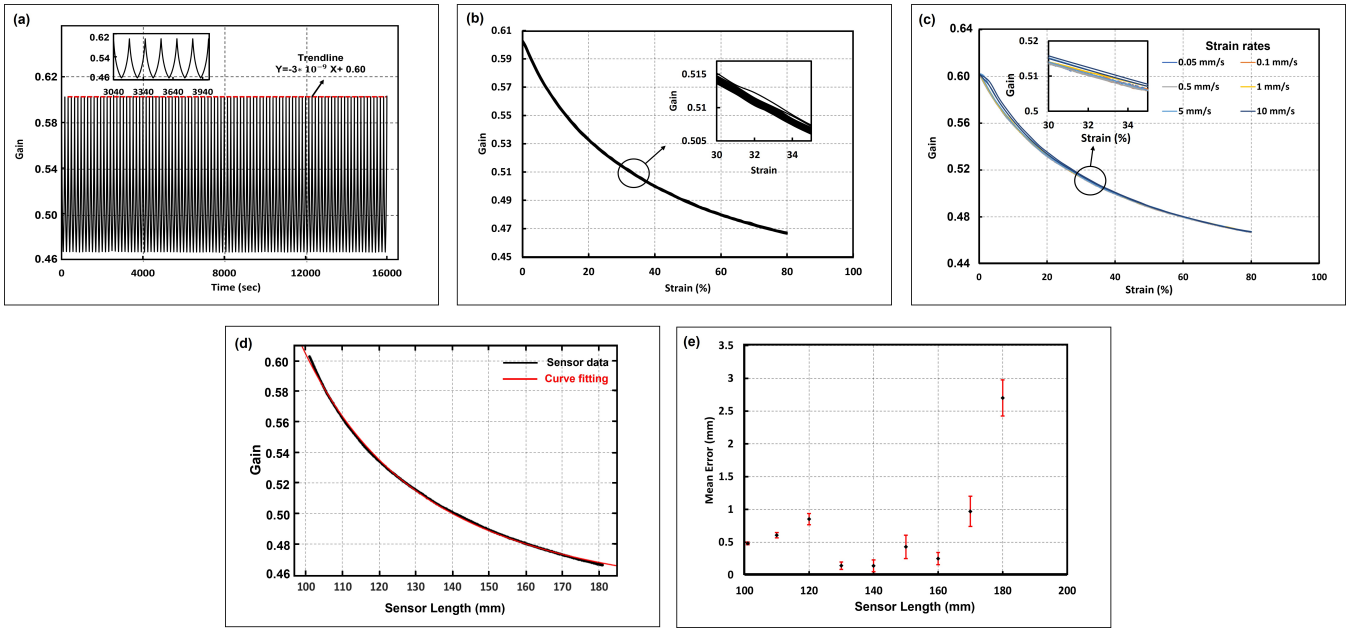

Fig. 5. (a) Gain change for repetitive loading; (b) electrical hysteresis for 100 cycles; (c) effect of strain rates on electrical hysteresis; (d) sensor calibration; (e) sensor accuracy.

C. Sensor calibration

The gain expression developed in section II is based on simple physics-based modeling of the sensor behavior. For calibration, a curve fitting approach was preferred to maximize the accuracy of the measurement. As the trend of the plot between gain and length data is non-linear, the linear curve fitting method was immediately rejected. Next, other curve-fitting basis functions with increasing complexity (inverse, polynomial, and power) were considered and compared in terms of R-square values. The best description is obtained with a power curve (Fig. 5d), as shown in equation (6), with a goodness of fit of 0.9994. This calibration is used for calculating the length in the remaining part of the paper.

$$l = \left(\frac{1.417 * 10^5}{G - 0.4395}\right)^{0.337} \tag{6}$$

D. Sensor precision and accuracy

For precision assessment, a known elongation was applied to the sensor for 15 times forward and 15 times backward using the linear motor stage. Then, the equation obtained by fitting the gain and length data from the previous process was used to estimate the length of the sensor. The calculated length data of 30 trials were utilized to find the percentage mean deviation among them. This was repeated for a series of nine different lengths, ranging between 100 and 180 mm, as shown in Table II. The maximum deviation observed was equal to 0.14%. The mean value obtained for each predefined spring length was finally compared to the reference value imposed by the setup. Fig. 5e shows the mean and standard deviation of the length estimation process that shows the maximum error at 80% strain. The average accuracy is 0.73 mm, which represents 0.9% of the applied strain. Compared to capacitive and resistive sensors [13], [42], this sensing method produces adequate precision and accuracy over an 80% deformation range.

TABLE II
PRECISION OF THE SENSOR

Elongation (mm)	Mean Deviation (%)
101	0.011
110	0.036
120	0.056
130	0.06
140	0.072
150	0.12
160	0.14
170	0.09
180	0.12

IV. SENSOR APPLICATION IN A SOFT ACTUATOR

As the first proof of concept, the sensor was integrated with a soft actuator prototype that can extend up to a strain of 80%. The design and manufacturing are based on the process presented in [43]. The pneumatic artificial muscle (PAM) considered here comprises two solid ends and an artificial muscle in the middle. The artificial muscle was fabricated using an expandable braided sleeve and a stretchable elastomeric cylindrical core made from silicone rubber. The architecture and different components of the soft module are depicted in Fig. 6a. The final assembled PAM had a diameter (ϕ_p) of 10 mm and a length (b_p) of 130 mm while contracted. Here, a similar configuration of the sensor given in Fig. 3b was prepared and integrated along the central axis of the PAM while both the ends were firmly connected to the solid ends using thread and superglue (Fig. 6b & c).

During the experiments, the PAM was inserted in a transparent cylindrical guide of diameter 12 mm and length 270 mm to restrict the actuator's movement to a single direction (Fig. 6d

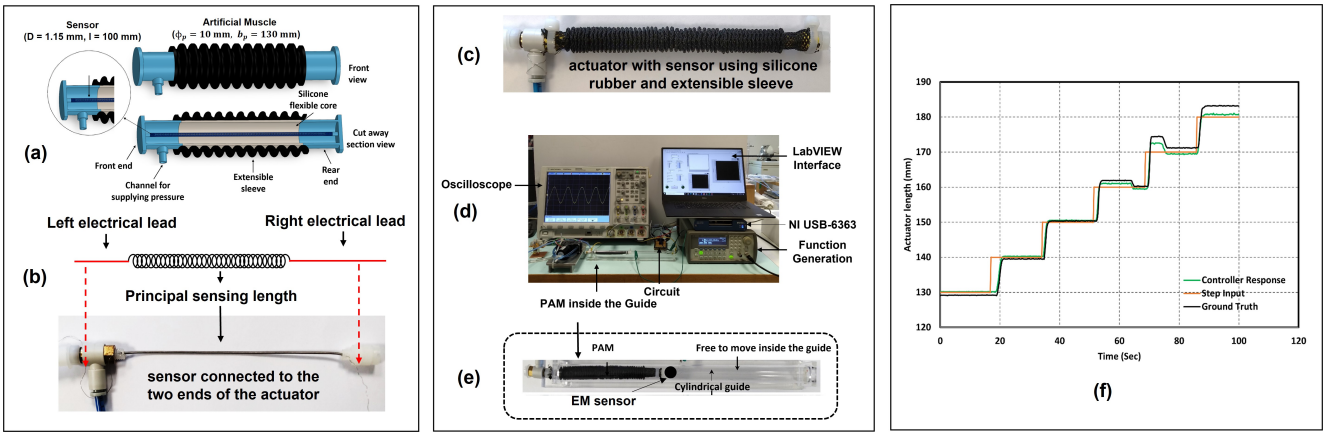

Fig. 6. (a) CAD design of PAM with different components; (b) sensor configuration; (c) sensor integration with the soft actuator; (d) different parts of P-controller; (e) PAM inside the guide; (f) comparison of the lengths estimated from the sensor with the ground truth values during position control.

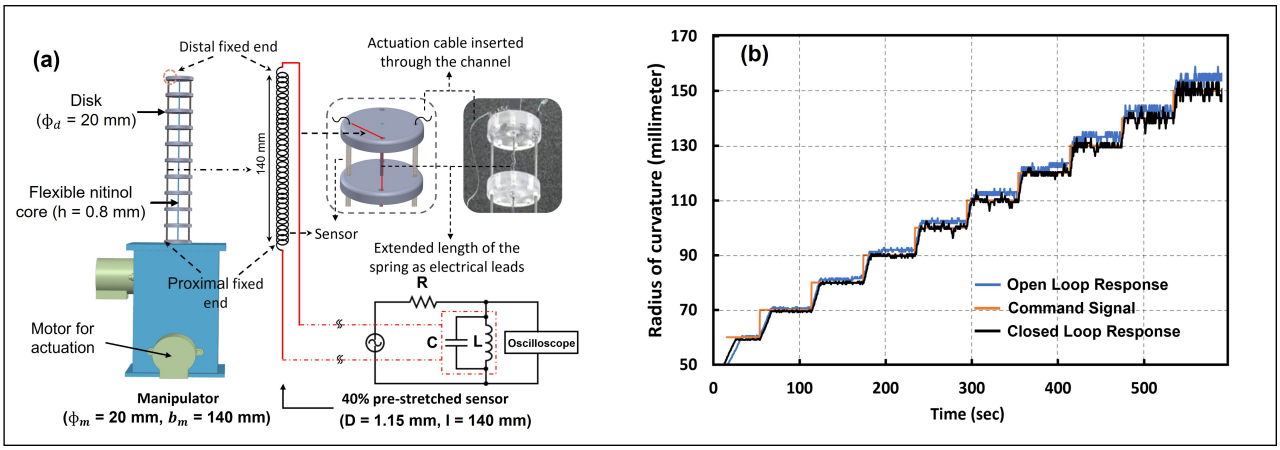

Fig. 7. (a) Tendon-driven manipulator and sensor integration process; (b) control of the radius of curvature of the manipulator using sensor information.

& e). In this setup, the left end of the actuator was fixed at the beginning of the guide while the other end was free to move. A proportional controller was designed to control the length of the soft actuator. It was implemented using LabVIEW in which the error signal was calculated using the desired length and feedback from the inductance sensor. The error signal was then processed inside the controller that generated an actuating signal that directed the PAM to move forward or backward based on the desired length.

The behavior of the soft actuator was assessed by exciting the system with a 10 mm step input at 20s-intervals from 130 mm, i.e., "0% strain of the sensor" to 180 mm, i.e., "50% strain of the sensor". Next, the length of the actuator was recorded by the sensor and compared with the length generated from the ground truth. In this case, one electromagnetic sensor (Aurora, NDI Digital, Canada) was used at the tip that provided the real length of the actuator with respect to the fixed base. The difference between the length of the actuator acquired by the sensor and the ground truth was estimated as 1.16 ± 0.75 mm (Fig. 6f). The closed-loop control shows that the sensor effectively controls the soft actuator with acceptable accuracy despite the absence of any physical model of PAM.

V. Sensor's Application in a Tendon-Driven Flexible Manipulator

Curvature estimation is a crucial process in the case of medical robots, such as follow-the-leader robot [44], common tendon-driven flexible robots [20], [45], and fluidic actuator [46]. This estimation can be used to either obtain the tip information [20] or reconstruct the shape [47] that can be used for precisely controlling or assisting the clinician during several minimally invasive surgical procedures. Thus, the sensor capability during curvature sensing was investigated by embedding into a prototype of the tendon-driven flexible manipulator. The prototype was fabricated using eleven cylindrical disks made of plexiglass. The design and fabrication followed the procedure presented in [48]. The disks were 20 mm in diameter (ϕ_d) and 3 mm in thickness. Moreover, the cylindrical disks had a central hole (h = 0.8 mm) and four channels (D = 1.15 mm) at the periphery (Fig. 7a). A flexible Nitinol wire of 0.8 mm diameter was used as the central core of the system where the disks were glued by maintaining a distance of 10.7 mm to each other. Two springs (Table 1: second column, initial D = 1.15 mm, and l = 100 mm) were embedded into two opposite channels of the manipulator by prestretching them to 40%. One of the springs was used as

a sensor while the other was intended to balance the tension forces. One interesting feature of these sensors is their easy integration. Here, the manipulator's design was only slightly modified to easily mount the springs simply by gluing their ends to the top disk. As shown in Fig. 7a, the extra helical coils of the spring were converted into straight configurations, which were further inserted through the other channels present in the manipulator, to connect to the circuit. Thanks to the hollow configuration of the springs, two cables were inserted inside the springs that were further connected to the motor, using a pulley for actuation. The length (b_m) and diameter (ϕ_m) of the manipulator are 140 mm and 20 mm, respectively. The detailed design and fabrication of the manipulator with the sensor are shown in Fig. 7a.

A PID controller was designed to control the radius of curvature of the flexible manipulator. This radius was estimated using a basic model, with a constant curvature assumption:

$$r = \frac{l_n}{\theta} \tag{7}$$

$$\theta = \frac{l_n - l_s}{a} \tag{8}$$

where l_n, r, and θ are the length of the neutral axis, radius of curvature, and angle of curvature of the manipulator, respectively, while l_s is the length of the sensor, and a is the distance from the central axis of the manipulator to the sensor.

In the literature, different curvature sensing solutions were presented for various medical robots performing bending radii ranging between 40 and 150 mm [45]–[47]. In some cases, a bending radius of 100 mm [45] is needed for approaching from the upper gastrointestinal tract to bypass the large organs. Considering these aspects, ten desired radii of curvature signals between 60 and 150 mm were selected. Next, each radius was applied for 60 sec, and the controller response was observed. For comparison, an open-loop control was performed using the cable length, and the results were compared with the control signals (Fig. 7b). The mean steady-state error in the case of the open-loop control was 5 mm, which is 3.6% of the length of the manipulator. On the other hand, for the closed-loop control, this error was 2 mm, i.e, 1.4% of the length of the manipulator. Therefore, it is possible to reduce the control error by 2.5, thanks to the sensor which is also convenient for integration from a hardware point of view.

VI. Conclusion

In this paper, the development of inductive sensing for flexible and soft robots was investigated. A method was proposed to optimize the measurement performance, using a simple P-P voltage instead of measuring the direct inductance. It indeed simplifies the required instrumentation and simultaneously adjusts the gain and sensitivity by tuning the circuit parameters. To avoid the sensor being device-specific, a single calibration curve was generated independently via the elongation mode that can be used in linear actuators and flexible manipulators. The characterization process shows that the sensor exhibits a low amount of hysteresis (0.1%), compared to resistive sensors [11], [12]. The sensor also had a precision in the order of 0.14% and an accuracy of 0.9%, which shows better performance with respect to some resistive and capacitive sensing technologies [13], [42]. Finally, in the first proof of concept, a model-free control could be implemented with a satisfying accuracy even at 50% strain. With the second proof of concept, the curvature control of a tendon-driven manipulator was demonstrated using the length information from the sensor. The sensor's performance in the two prototypes shows that it can be easily integrated with a high level of compactness. Moreover, it can measure both linear and bending strain using a single calibration curve generated externally. However, to differentiate between the bending and linear elongation strain, multiple sensors are needed in the same way, followed by other sensing technologies. Due to the small size and low stiffness (6.5 mN/mm) of the sensors, they can become interesting solutions for integration in miniature soft and flexible manipulators. In this study, two springs of the same length and different diameters have been experimentally tested. In the general case, a mechatronic design approach can be used to select the sensor geometry, such as length and diameter, to optimize measurement conditions under specific design constraints for a given manipulator. It should be highlighted that an excessive reduction in length and diameter may reduce the gain change and signal-to-noise ratio, which may require more precise instrumentation for measurement. Moreover, the model adopted in the methodology neglects the effect of relative permeability, the internal resistance of the spring and connecting wires, and the changes in the pitch and diameter of the spring. Taking into account these parameters will be the object of future work to enhance the optimization process. In particular, if the spring coil shape is not maintained, a correction factor to handle the evolution of geometry would need to be identified. Other spring materials, such as copper and nitinol will also be studied.

Here, the sensor is used to sense only the bending or elongation. However, in some applications, the body of soft robots is subjected to twisting. Thus, the design of the sets of inductive sensors to assess the bending, elongation, and twisting of soft robots will be of great interest too. The exploitation of spring tension as a prestress element used in the design of flexible manipulators will be another direction of development.

In this paper, the sensor was used for the curvature sensing and control of the flexible robot that will help the robot to reach hard-to-reach locations. Sometimes, the shape information of the robots is highly important to precisely control the robot inside the anatomy by avoiding collision with healthy tissue. Thus, future work will go beyond the curvature control to estimate the pose of medical manipulators by fusing sensory information with the existing kinematic models. The proposed sensing solution is not only limited to medical robots, but may also be considered to extract the shape in other contexts like tensegrity mechanism control [49] or human body reconstruction [50]. In such cases, multiple sensors with machine learning or neural network methods might be adapted to tackle the complexity and the procedures established in [49], [50] could be followed.

ACKNOWLEDGMENT

The authors wish to thank the ATLAS project team; in particular Dr. Veronica Iacovacci, Dr. Selene Tognarelli, and Mohammad Hasan Dad Ansari from the BioRobotics Institute, Scuola Superiore Sant'Anna for fruitful discussions to develop the manuscript. They also thank Dr. Linda Paternò for the support in the development of the actuator.

REFERENCES

[1] I. De Falco, M. Cianchetti, and A. Menciassi, "A soft multi-module manipulator with variable stiffness for minimally invasive surgery," Bioinspiration & Biomimetics, vol. 12, no. 5, p. 56008, Sep. 2017, doi: 10.1088/1748-3190/aa7ccd.

[2] T. Ranzani, G. Gerboni, M. Cianchetti, and A. Menciassi, "A bioinspired soft manipulator for minimally invasive surgery," Bioinspiration & Biomimetics, vol. 10, no. 3, p. 35008, 2015, doi: 10.1088/1748-3190/10/3/035008.

[3] I. Tamadon, G. Soldani, P. Dario and A. Menciassi, "Novel Robotic Approach for Minimally Invasive Aortic Heart Valve Surgery," 2018 40th Annual International Conference of the IEEE Engineering in Medicine and Biology Society (EMBC), 2018, pp. 3656-3659, doi: 10.1109/EMBC.2018.8513309.

[4] M. D. M. Kutzer, S. M. Segreti, C. Y. Brown, M. Armand, R. H. Taylor and S. C. Mears, "Design of a new cable-driven manipulator with a large open lumen: Preliminary applications in the minimally-invasive removal of osteolysis," 2011 IEEE International Conference on Robotics and Automation, 2011, pp. 2913-2920, doi: 10.1109/ICRA.2011.5980285.

[5] H. Wang, M. Totaro, and L. Beccai, "Toward Perceptive Soft Robots: Progress and Challenges," Advanced Science, vol. 5, no. 9, p. 1800541, 2018, doi: https://doi.org/10.1002/advs.201800541.

[6] A. Koivikko, E. Sadeghian Raei, M. Mosallaei, M. Mäntysalo and V. Sariola, "Screen-Printed Curvature Sensors for Soft Robots," in IEEE Sensors Journal, vol. 18, no. 1, pp. 223-230, 1 Jan.1, 2018.

[7] S. Russo, T. Ranzani, H. Liu, S. Nefti-Meziani, K. Althoefer, and A. Menciassi, "Soft and Stretchable Sensor Using Biocompatible Electrodes and Liquid for Medical Applications," Soft Robot., vol. 2, no. 4, pp. 146–154, 2015, doi: 10.1089/soro.2015.0011.

[8] Y. Park and R. J. Wood, "Smart pneumatic artificial muscle actuator with embedded microfluidic sensing," SENSORS, 2013 IEEE, 2013, pp. 1-4, doi: 10.1109/ICSENS.2013.6688298.

[9] E. L. White, J. C. Case, and R. K. Kramer, "Multi-mode strain and curvature sensors for soft robotic applications," Sensors and Actuators A: Physical, vol. 253, pp. 188–197, 2017, doi: https://doi.org/10.1016/j.sna.2016.11.031.

[10] T. Helps, and J. Rossiter, "Proprioceptive flexible fluidic actuators using conductive working fluids." Soft robotics 5.2 (2018): 175-189.

[11] X. Tang, K. Li, Y. Liu and J. Zhao, "Coiled Conductive Polymer Fiber Used in Soft Manipulator as Sensor," in IEEE Sensors Journal, vol. 18, no. 15, pp. 6123-6129, 1 Aug.1, 2018, doi: 10.1109/JSEN.2018.2846553.

[12] M. Cianchetti, F. Renda, A. Licofonte, and C. Laschi, "Sensorization of continuum soft robots for reconstructing their spatial configuration," in 2012 4th IEEE RAS & EMBS International Conference on Biomedical Robotics and Biomechatronics (BioRob), 2012, pp. 634–639, doi: 10.1109/BioRob.2012.6290788.

[13] H. Nakamoto et al., "Application of stretchable strain sensor for pneumatic artificial muscle," in 2014 IEEE Symposium on Robotic Intelligence in Informationally Structured Space (RiiSS), 2014, pp. 1–5, doi: 10.1109/RIISS.2014.7009179.

[14] M. C. Yuen, R. Kramer-Bottiglio, and J. Paik, "Strain sensor-embedded soft pneumatic actuators for extension and bending feedback," in 2018 IEEE International Conference on Soft Robotics (RoboSoft), 2018, pp. 202–207, doi: 10.1109/ROBOSOFT.2018.8404920.

[15] M. C. Yuen, H. Tonoyan, E. L. White, M. Telleria, and R. K. Kramer, "Fabric sensory sleeves for soft robot state estimation," in 2017 IEEE International Conference on Robotics and Automation (ICRA), 2017, pp. 5511–5518, doi: 10.1109/ICRA.2017.7989649.

[16] J. Legrand, B. Loenders, A. Vos, L. Schoevaerdts and E. Vander Poorten, "Integrated Capacitance Sensing for Miniature Artificial Muscle Actuators," in IEEE Sensors Journal, vol. 20, no. 3, pp. 1363-1372, 1 Feb.1, 2020, doi: 10.1109/JSEN.2019.2946268.

[17] O. Atalay, "Textile-Based, Interdigital, Capacitive, Soft-Strain Sensor for Wearable Applications," Materials (Basel)., vol. 11, no. 5, 2018, doi: 10.3390/ma11050768.

[18] T. C. Searle, K. Althoefer, L. Seneviratne and H. Liu, "An optical curvature sensor for flexible manipulators," 2013 IEEE International Conference on Robotics and Automation, 2013, pp. 4415-4420, doi: 10.1109/ICRA.2013.6631203.

[19] S. Sareh, Y. Noh, M. Li, T. Ranzani, H. Liu, and K. Althoefer, "Macrobend optical sensing for pose measurement in soft robot arms," Smart Materials and Structures 24, no. 12 (2015), doi: 10.1088/0964-1726/24/12/125024.

[20] R. J. Roesthuis, S. Janssen, and S. Misra, "On using an array of fiber Bragg grating sensors for closed-loop control of flexible minimally invasive surgical instruments," in 2013 IEEE/RSJ International Conference on Intelligent Robots and Systems, 2013, pp. 2545–2551, doi: 10.1109/IROS.2013.6696715.

[21] X. Zhou, S. Li, X. Li, X. Yan, X. Zhang and T. Cheng, "A Vectorial Analysis of the Curvature Sensor Based on a Dual-Core Photonic Crystal Fiber," in IEEE Transactions on Instrumentation and Measurement, vol. 69, no. 9, pp. 6564-6570, Sept. 2020, doi: 10.1109/TIM.2020.2968777.

[22] J. Feng, Y. Zhao, X.-W. Lin, W. Hu, F. Xu, and Y.-Q. Lu, "A Transflective Nano-Wire Grid Polarizer Based Fiber-Optic Sensor," Sensors, vol. 11, no. 3, pp. 2488–2495, 2011, doi: 10.3390/s110302488.

[23] W. Zhuang, G. Sun, H. Li, X. Lou, M. Dong, and L. Zhu, "FBG based shape sensing of a silicone octopus tentacle model for soft robotics," Optik (Stuttg)., vol. 165, pp. 7–15, 2018, doi: https://doi.org/10.1016/j.ijleo.2018.03.087.

[24] J. Wei, S. Wang, J. Li and S. Zuo, "Novel Integrated Helical Design of Single Optic Fiber for Shape Sensing of Flexible Robot," in IEEE Sensors Journal, vol. 17, no. 20, pp. 6627-6636, 15 Oct.15, 2017, doi: 10.1109/JSEN.2017.2748162.

[25] S. Sefati, R. Hegeman, F. Alambeigi, I. Iordachita, and M. Armand, "FBG-Based Position Estimation of Highly Deformable Continuum Manipulators: Model-Dependent vs. Data-Driven Approaches," in 2019 International Symposium on Medical Robotics (ISMR), 2019, pp. 1–6, doi: 10.1109/ISMR.2019.8710179.

[26] Y. He, X. Zhang, L. Zhu, G. Sun, X. Lou, and M. Dong, "Optical Fiber Sensor Performance Evaluation in Soft Polyimide Film with Different Thickness Ratios," Sensors, vol. 19, no. 4, 2019, doi: 10.3390/s19040790.

[27] S. K. Sahu, C. Sozer, B. Rosa, I. Tamadon, P. Renaud, and A. Menciassi, "Shape Reconstruction Processes for Interventional Application Devices: State of the Art, Progress, and Future Directions," Frontiers in Robotics and AI 8 (2021), doi: 10.3389/frobt.2021.758411.

[28] J.-M. Kim, C.-M. Kim, S.-Y. Choi, and B. Y. Lee, "Enhanced Strain Measurement Range of an FBG Sensor Embedded in Seven-Wire Steel Strands," Sensors, vol. 17, no. 7, 2017, doi: 10.3390/s17071654.

[29] R. Liu, S. Wang, H. Yang and C. Shi, "Highly Stretchable Strain Sensor With Spiral Fiber for Curvature Sensing of a Soft Pneumatic Gripper," in IEEE Sensors Journal, vol. 21, no. 21, pp. 23880-23888, 1 Nov.1, 2021, doi: 10.1109/JSEN.2021.3116427.

[30] Z. Xing, J. Lin, D. McCoul, D. Zhang, and J. Zhao, "Inductive Strain Sensor With High Repeatability and Ultra-Low Hysteresis Based on Mechanical Spring," in IEEE Sensors Journal, vol. 20, no. 24, pp. 14670-14675, 15 Dec.15, 2020, doi: 10.1109/JSEN.2020.3010345.

[31] W. Felt, K. Y. Chin and C. D. Remy, "Contraction Sensing With Smart Braid McKibben Muscles," in IEEE/ASME Transactions on Mechatronics, vol. 21, no. 3, pp. 1201-1209, June 2016, doi: 10.1109/TMECH.2015.2493782.

[32] W. Felt et al., "An inductance-based sensing system for bellows-driven continuum joints in soft robots," Auton. Robots, vol. 43, no. 2, pp. 435–448, 2019, doi: 10.1007/s10514-018-9769-7.

[33] A. R. Plamootil Mathai, T. Stalin and P. Valvivia y Alvarado, "Flexible Fiber Inductive Coils for Soft Robots and Wearable Devices," in IEEE Robotics and Automation Letters, vol. 7, no. 2, pp. 5711-5718, April 2022, doi: 10.1109/LRA.2022.3159864.

[34] A. Fassler, and C. Majidi. "Soft-matter capacitors and inductors for hyperelastic strain sensing and stretchable electronics." Smart Materials and Structures 22.5 (2013): 055023.

[35] S. Hamaguchi et al., "Soft Inductive Tactile Sensor Using Flow-Channel Enclosing Liquid Metal," in IEEE Robotics and Automation Letters, vol. 5, no. 3, pp. 4028-4034, July 2020, doi: 10.1109/LRA.2020.2985573.

[36] O. Azami, D. Morisaki, T. Miyazaki, T. Kanno, and K. Kawashima, "Development of the extension type pneumatic soft actuator with built-in displacement sensor," Sensors Actuators A: Physical, vol. 300, p. 111623, 2019, doi: https://doi.org/10.1016/j.sna.2019.111623.

[37] A. V. Prituja, H. Banerjee and H. Ren, "Electromagnetically Enhanced Soft and Flexible Bend Sensor: A Quantitative Analysis With Different Cores," in IEEE Sensors Journal, vol. 18, no. 9, pp. 3580-3589, 1 May1, 2018, doi: 10.1109/JSEN.2018.2817211.

[38] K. Choi, S. J. Park, M. Won, and C. H. Park, "Soft Inductive Coil Spring Strain Sensor Integrated with SMA Spring Bundle Actuator," Sensors, vol. 21, no. 7, p. 2304, Mar. 2021, doi: 10.3390/s21072304.

[39] J. Jeon and C. Kim, "Shape Sensor Using Magnetic Induction with Frequency Sweeping for Medical Catheters," 2021 IEEE International Conference on Robotics and Automation (ICRA), 2021, pp. 7137-7143, doi: 10.1109/ICRA48506.2021.9561072.

[40] Q. Yu and T. W. Holmes, "Stray capacitance modeling of inductors by using the finite element method," in 1999 IEEE International Symposium on Electromagnetic Compatability. Symposium Record (Cat. No.99CH36261), 1999, vol. 1, pp. 305–310 vol.1, doi: 10.1109/ISEMC.1999.812918.

[41] A. Massarini and M. K. Kazimierczuk, "Self-capacitance of inductors," in IEEE Transactions on Power Electronics, vol. 12, no. 4, pp. 671-676, July 1997, doi: 10.1109/63.602562.

[42] V. A. Ho and S. Hirai, "Measuring McKibben actuator shrinkage using fiber sensor," in 2015 24th IEEE International Symposium on Robot and Human Interactive Communication (RO-MAN), 2015, pp. 628–633, doi: 10.1109/ROMAN.2015.7333585.

[43] T. Yukisawa, Y. Ishii, S. Nishikawa, R. Niiyama, and Y. Kuniyoshi, "Modeling of extensible pneumatic actuator with bellows (EPAB) for continuum arm," in 2017 IEEE International Conference on Robotics and Biomimetics (ROBIO), 2017, pp. 2303–2308, doi: 10.1109/ROBIO.2017.8324762.

[44] M. Neumann and J. Burgner-Kahrs, "Considerations for follow-the-leader motion of extensible tendon-driven continuum robots," 2016 IEEE International Conference on Robotics and Automation (ICRA), 2016, pp. 917-923, doi: 10.1109/ICRA.2016.7487223.

[45] J. Wei, S. Wang, J. Li and S. Zuo, "Novel Integrated Helical Design of Single Optic Fiber for Shape Sensing of Flexible Robot," in IEEE Sensors Journal, vol. 17, no. 20, pp. 6627-6636, 15 Oct.15, 2017, doi: 10.1109/JSEN.2017.2748162.

[46] Y. He, L. Zhu, G. Sun, M. Yu, and M. Dong, "Design, Measurement and Shape Reconstruction of Soft Surgical Actuator Based on Fiber Bragg Gratings," Applied Sciences, vol. 8, no. 10, p. 1773, Sep. 2018, doi: 10.3390/app8101773.

[47] X. Yi, J. Qian, L. Shen, Y. Zhang and Z. Zhang, "An Innovative 3D Colonoscope Shape Sensing Sensor Based on FBG Sensor Array," 2007 International Conference on Information Acquisition, 2007, pp. 227-232, doi: 10.1109/ICIA.2007.4295731.

[48] D. C. Rucker and R. J. Webster III, "Statics and Dynamics of Continuum Robots With General Tendon Routing and External Loading," in IEEE Transactions on Robotics, vol. 27, no. 6, pp. 1033-1044, Dec. 2011, doi: 10.1109/TRO.2011.2160469.

[49] W. -Y. Li, A. Takata, H. Nabae, G. Endo and K. Suzumori, "Shape Recognition of a Tensegrity With Soft Sensor Threads and Artificial Muscles Using a Recurrent Neural Network," in IEEE Robotics and Automation Letters, vol. 6, no. 4, pp. 6228-6234, Oct. 2021, doi: 10.1109/LRA.2021.3091384.

[50] Z. Chen, R. Wu, S. Guo, X. Liu, H. Fu, X. Jin, and M. Liao, "3D upper body reconstruction with sparse soft sensors," Soft Robotics, 2021, 8(2), 226-239, doi: 10.1089/soro.2019.0187.